Higher-Symmetries for Broadband Reflecting Luneburg Lenses at Ka-band

C. Bilitos, J. Ruiz-Garcia, R Sauleau, E Martini, S. Maci, D. Gonzalez-Ovejero

Higher-Symmetries for Broadband Reflecting Luneburg Lenses at Ka-band

C. Bilitos*, J. Ruiz-García*, R. Sauleau*, E. Martini†, S. Maci † and D. González-Ovejero *
*Univ. Rennes, CNRS, IETR (Institut d'Electronique et des Technologies du numéRique) - UMR 6164, F-35000, Rennes, France , christos.bilitos@univ-rennes1.fr
†Department of Information Engineering and Mathematics, University of Siena, 53100, Siena, Italy, macis@dii.unisi.it

***Abstract*—This paper reports the application of higher symmetries to the design of a Reflecting Luneburg Lens (RLL) with broadband response. RLLs consist of two circular parallel plate waveguides (PPWs) vertically stacked. The bottom PPW is filled with an azimuthally symmetric graded index (GRIN) medium. Owing to this GRIN medium, the wave launched by a primary feed in the bottom PPW is collimated in the top one, so that a plane wave with a different propagation direction is generated for any azimuthal position of the source. In this work, the GRIN medium in the bottom PPW is implemented by higher symmetry unit-cells consisting of metallic inclusions. This type of unit-cell achieves the required effective refractive index profile with reduced frequency dispersion, thus increasing the operational bandwidth of the lens. The proposed architecture constitutes a low-profile beam-forming solution that also provides complete azimuthal scanning in a wide frequency range. Moreover, it remains completely metallic, thus benefitting from structural robustness and reduced losses.**

***Index Terms*—Metasurface, Reflecting Luneburg Lens, beam-forming, higher symmetries, Ka-band, planar antennas.**

I. Introduction

Future wireless communications will demand higher data rates and, therefore, broader bandwidths (BWs). This need has fostered the interest in accessing higher frequency bands and, in particular, the Ka-band [1]. The complexity and cost of phased arrays at this band may limit their application in certain scenarios. Quasi-optical (QO) systems in parallel plate waveguide (PPW) provide an alternative compact and low-cost solution for multi beam antennas and, thus, for scanning by beam switching in this band. Among QO beam-formers, one finds pillbox systems [2], which consist of double-layered PPW structures with a 180° PPW bend of parabolic profile connecting the bottom and top PPW. In these structures, multiple pencil beams are obtained owing to the radiating aperture in the top layer. However, the azimuthal scanning will be limited by coma phase errors due to the parabolical reflector. Flat Luneburg lenses (LLs) [3] are another popular solution where fan beams are generated providing azimuthal scanning, only limited by the number of sources.

An alternative to pillbox QO beamformers, recently introduced in [4] is the Reflecting Luneburg lens (RLL). This new lens comprises two stacked circular PPWs. The bottom PPW is filled with a graded index (GRIN) medium, which guides the rays launched by a source in the focal circumference along curvilinear paths. After reflection and coupling to the upper PPW, the rays emerge parallel in the azimuthal direction given by the source position. RLLs constitute a compact QO beam-former, that mitigates the scanning limitations of classical pillbox systems. However, the implementation of the RLL's GRIN medium requires a refractive index range larger than the one found in the LL. Therefore, finding an appropriate unit-cell to realize a broadband RLL can be challenging. The concept of mirroring and transposing the unit-cell geometry was first introduced in the 60's and 70's [5], [6] and recently revisited in [7] for the implementation of broadband Luneburg lenses. In this work, we explore the use of unit-cells with higher symmetries for the design of a broadband RLL.

II. Reflecting Luneburg Lens Implementation

As mentioned, RLLs comprise two stacked PPWs where the bottom one is loaded by a GRIN medium. When fed from its focal circumference, the rays in the bottom PPW follow curvilinear paths (shown in Fig. 1(a)), so that after reflection on a PEC boundary a planar wavefront is coupled to the upper layer. The refractive index profile of the GRIN medium [4], is given by:

$$n(r) = n_0 \left(\frac{-1 + \sqrt{1 + 8(r/R)^2}}{2\left((r/R)^2\right)} \right)^{3/2} \tag{1}$$

where n_0 is the refractive index of free space, r is the radial distance and R is the radius of the lens. For the efficient coupling of the wavefronts to the air-filled top PPW a corner reflector can be employed, as the refractive index at the rim of the lens is equal to n_0.

The aforementioned ray-paths inside the GRIN medium present an additional and quite interesting property. Other than the focal region residing in the focal circumference of the lens, a second internal focal region can be noticed inside the GRIN medium around a radial distance of $r = 0.46R$. It has been shown in [4] that the source can be placed directly in the inner focal region of the lens without significantly changing its behavior (Fig. 1(b)). This property is of crucial importance in practical scenarios as the source and the corner reflector no longer coexist in the focal circumference. This way, one avoids undesired coupling and increases the azimuthal scanning range. This study focuses on the realization of the lower layer GRIN medium and the coupling with the upper PPW for the original RLL design as well as its internal focal region variation.

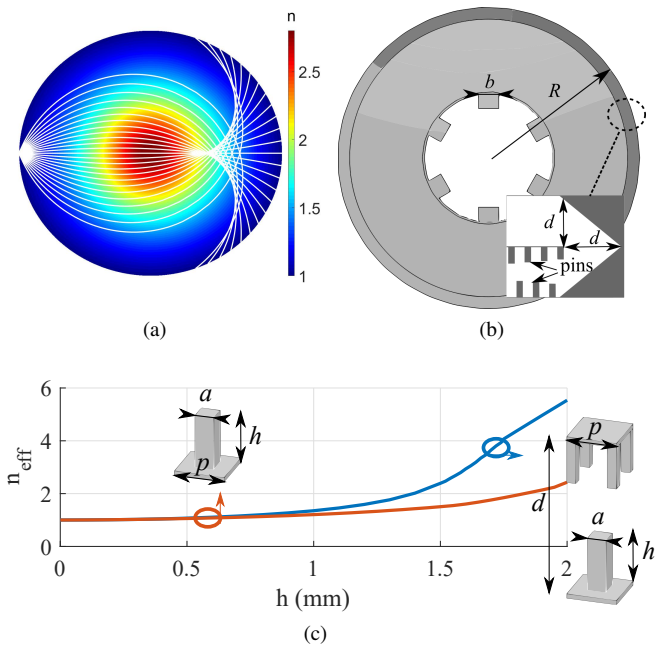

Fig. 1. (a) Ray-paths in the RLL's GRIN medium. (b) Top view of the bottom layer of the RLL, utilizing the internal focal region and side view of the corner reflector used to couple the power to the upper PPW. (c) Local effective refractive index as a function of post height at 30 GHz for unit-cell with higher symmetries (blue) and conventional unit-cell (orange), the post dimensions are a = 0.3 mm, p = 0.8 mm and d = 3 mm in both cases.

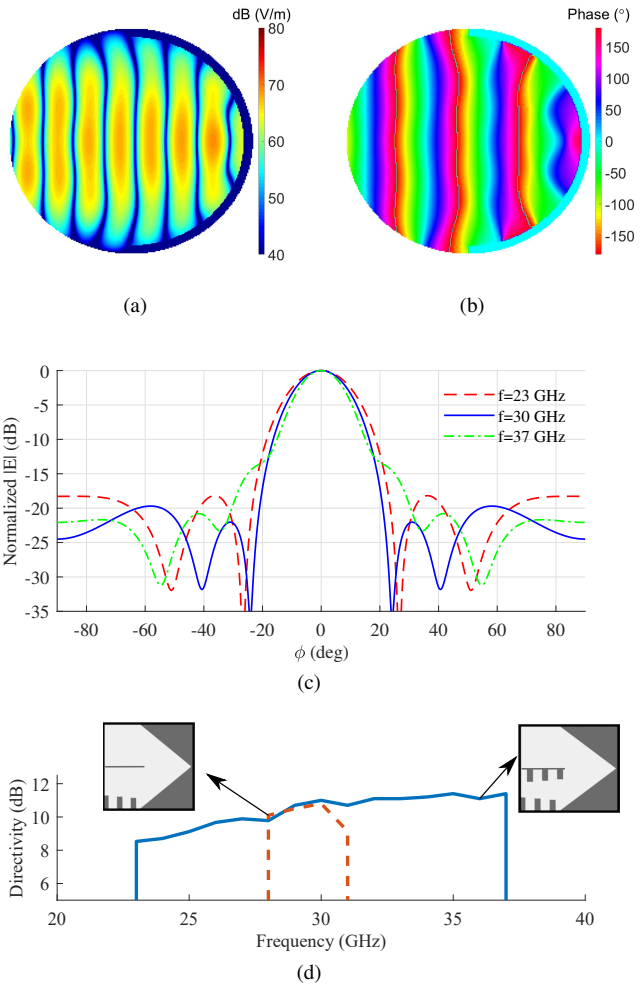

Fig. 2. (a) Real part of the vertical component of the electric field $Re(E_z)$ in logarithmic scale and (b) Phase distribution in degrees on the top PPW ($R = 2\lambda_0$). (c) Simulated H-plane radiation pattern for the central frequency $f_0 = 30$ GHz and the lower and upper limit of the operation band $f_l = 23$ GHz and $f_u = 37$ GHz. (d) Operational bandwidth comparison between RLL implementation with higher symmetries (solid blue line) and without (dashed orange line).

The RLL presents a maximum refractive index ($n_{max} = 2.82$ derived from (1)), substantially increased with respect to other GRIN lenses such as the Luneburg Lens ($n_{max} = 1.41$) and the Maxwell Fish-eye Lens ($n_{max} = 2$). This high variation limits the variety of unit-cells able to implement the RLL, especially if we want to maintain an all-metal design [8]. A metallic post structure is a promising candidate to implement this large refractive index range. However, when using such a structure to implement the RLL refractive index profile, we have to deal with a narrow stop band and the frequency dispersion of the metallic posts. This significantly reduces the frequency range with uni-modal propagation of the fundamental TM mode, necessary to avoid coupling to higher order modes. We can employ unit-cells with higher symmetries, to obtain large variations of the effective refracting index, while also mitigating the dispersive frequency behaviour on a wide frequency range. The unit-cells with higher symmetry are obtained by mirroring and transposing the initial unit-cell geometry. Since we aim at using a metal-only unit-cell, two solutions seem most suitable: higher symmetric metallic posts and their complementary higher symmetric holey structures. Although the holey unit-cell might appear as a more appealing solution due to its easier fabrication, acquiring the required refractive index range is challenging without dielectric loading [9]. Hence, we have concentrated our efforts on the metallic posts with higher symmetry.

Fig. 1(c) illustrates the proposed unit-cell geometry along with the effective refractive index variation obtained at 30 GHz by varying the post height h (solid blue line) compared with the conventional unit-cell (solid orange line). A variation of h between 0 and 2 mm suffices to implement $n(r)$ in (1). The other dimensions of the metallic inclusion are $a = 0.3$ mm, $p = 0.8$ mm and $d = 3$ mm. Finally, the side view of the corner reflector with the unit-cells are depicted on the right inset of Fig. 1(b).

III. Numerical Results

As proofs of the concept, two designs that exploit the proposed architecture have been analyzed by CST simulation software [10]. In the first case, the stacked circular PPWs comprising the design have a radius of $R = 2\lambda_0$, where λ_0 is the free-space wavelength at 30 GHz. The two plates forming the bottom PPW are loaded with the higher symmetry metallic unit-cell showcased in Section II. The lens area is divided using a Cartesian lattice with periodicity equal to the unit-cell

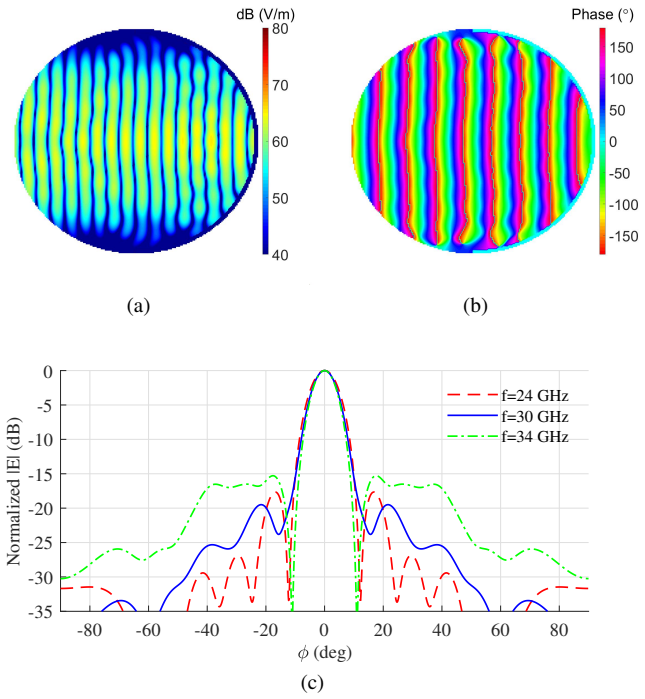

Fig. 3. (a) Real part of the vertical component of the electric field $Re(E_z)$ in logarithmic scale and (b) Phase distribution in degrees on the top PPW ($R = 4.5\lambda_0$). (c) Simulated H-plane radiation pattern for the central frequency $f_0 = 30$ GHz and the lower and upper limit of the operation band $f_l = 24$ GHz and $f_u = 34$ GHz.

side. Each cell is then filled with the post dimensions that match the local refractive index. The bottom and top PPWs present a height $d = 3$mm and they are connected by the corner reflector in the inset of Fig. 1(b). The system is fed from its focal circumference by an H-plane sectoral horn, with $b = 8.6$ mm and radiates through an aperture situated on the top PPW.

At the central frequency, the electric field in the top PPW in Fig. 2(a) shows a propagating plane wave, also demonstrated by the flatness of the field's phase distribution in Fig. 2(b). For the determination of the lens' bandwidth we consider the H-plane directivity within the -3 dB range presenting SLLs bellow -15 dB. Fig. 2(c) shows the calculated far-field patterns, which present a clear main lobe and low side lobe levels (SLLs) from 23 GHz up to 37 GHz (relative $BW \approx 47\%$). If one implements a RLL with the same radius using a conventional metal post unit-cell with identical sampling and side, the obtained operational bandwidth is reduced to just $\approx 10\%$. The directivity versus frequency response with SLLs bellow -15 dB for the two structures is presented in Fig. 2(d).

In the second case, the design fed from the internal focal region was evaluated for a upper and lower PPW radius of $R = 4.5\lambda_0$. The feed horn ($b = 6$ mm) is located in the internal focal region, at a radial distance $r = 0.46 * R$. In this region of the bottom PPW, in order to maintain sufficient space between the top and the bottom metallic posts for the introduction of the feed, the unit-cell dimensions of Section II were modified to $a = 0.5$ mm, $p = 1.1$ mm and $d = 3.5$ mm. The structure, operating at the central frequency, displays a plane wave in the top PPW, presented in Fig. 3(a) and Fig. 3(b). The calculated far-field pattern, depicted in Fig. 3(c), demonstrates a narrower main lobe with slightly increased SLLs, the operating bandwidth of the lens ranges from 24 GHz to 34 GHz (relative $BW \approx 35\%$). In comparison, the same structure implemented with the more conventional metal post unit-cell reports a relative $BW \approx 21\%$.

IV. Conclusions

In conclusion, higher symmetries have been applied to the realization of RLLs at Ka-band. Two different designs have been presented and validated by full-wave simulations, demonstrating the objective broadband performance. More specifically, the original RLL design and its internal focal region variation displayed a $BW \approx 47\%$ and $BW \approx 35\%$ respectively. The bandwidth decrease in the latter case is attributed to the modification of the unit-cell and the overall size of the structure. The final lens structure can be used as broadband beamformer at Ka-band providing full azimuthal scanning. Furthermore, the structure is compact and fully metallic, thus maintaining structural robustness and reduced losses.

Acknowledgements

This work has been supported by the Agence de l'Innovation de Défense (AID), and by the European Union through the European Regional Development Fund (ERDF), the French Region of Brittany, Ministry of Higher Education and Research, Rennes Métropole and Conseil Départemental 35, through the CPER Project STIC & Ondes.

References

[1] T. S. Rappaport, S. Sun, R. Mayzus, H. Zhao, Y. Azar, K. Wang, G. N. Wong, J. K. Schulz, M. Samimi, and F. Gutierrez, "Millimeter wave mobile communications for 5G cellular: It will work!" *IEEE Access*, vol. 1, pp. 335–349, 2013.

[2] M. Ettorre, R. Sauleau, and L. Le Coq, "Multi-beam multi-layer leaky-wave SIW pillbox antenna for millimeter-wave applications," *IEEE Trans. Antennas Propag.*, vol. 59, no. 4, pp. 1093–1100, Apr. 2011.

[3] F. Doucet, N. J. Fonseca, E. Girard, X. Morvan, L. Le Coq, H. Legay, and R. Sauleau, "Shaped continuous parallel plate delay lens with enhanced scanning performance," *IEEE Trans. Antennas Propag.*, vol. 67, no. 11, pp. 6695–6704, Nov. 2019.

[4] J. Ruiz-García, E. Martini, C. D. Giovampaola, D. González-Ovejero, and S. Maci, "Reflecting Luneburg lenses," *IEEE Trans. Antennas Propag.*, vol. 69, no. 7, pp. 3924–3935, Jul. 2021.

[5] P. Crepeau and P. McIsaac, "Consequences of symmetry in periodic structures," *Proc. IEEE*, vol. 52, no. 1, pp. 33–43, 1964.

[6] A. Hessel, Ming Hui Chen, R. Li, and A. Oliner, "Propagation in periodically loaded waveguides with higher symmetries," *Proc. IEEE*, vol. 61, no. 2, pp. 183–195, 1973.

[7] O. Quevedo-Teruel, M. Ebrahimpouri, and M. N. M. Kehn, "Ultrawideband metasurface lenses based on off-shifted opposite layers," *IEEE Antennas Wirel. Propag. Lett.*, vol. 15, pp. 484–487, Dec. 2016.

[8] D. González-Ovejero, N. Chahat, R. Sauleau, G. Chattopadhyay, S. Maci, and M. Ettorre, "Additive manufactured metal-only modulated metasurface antennas," *IEEE Trans. Antennas Propag.*, vol. 66, no. 11, pp. 6106–6114, Nov. 2018.

[9] G. Valerio, F. Ghasemifard, Z. Sipus, and O. Quevedo-Teruel, "Glide-symmetric all-metal holey metasurfaces for low-dispersive artificial materials: Modeling and properties," *IEEE Trans. Microw. Theory Tech.*, vol. 66, no. 7, pp. 3210–3223, Jul. 2018.

[10] CST of America, "CST Microwave Studio," Anaheim, CA, 2020.